Short Communication

Analysis of standing-wave stack for direct cooling and orthoparahydrogen conversion of cryogenic hydrogen

Konstantin I. Matveev¹, Jacob W. Leachman

Hydrogen Properties for Energy Research (HYPER) Laboratory, School of Mechanical and Materials Engineering, Washington State University, Pullman, WA, 99164, USA

Abstract

Direct cooling of cryogenic hydrogen can be achieved by flow through a stack or regenerator of a thermoacoustic refrigerator. In addition, using a catalytic stack, the ortho-parahydrogen transformation can be conveniently realized in the same device. Analysis of this system element is carried out by integrating one-dimensional thermoacoustic equations with addition of empirical ortho-parahydrogen conversion reaction. Calculations in a standing-wave catalyzed setup demonstrate a selection process for optimal acoustic impedance and stack pore dimensions, showing significant advantage over non-catalyzed hydrogen- and helium-based stacks of similar kind. Results are presented for hydrogen flow characteristics and distributed heat load due to ortho-parahydrogen conversion inside a stack. The stack performance is also quantified at variable flow rate of hydrogen, stack length, mean pressure, and supplied acoustic power.

Keywords: standing-wave refrigerator, cryogenic cooling, ortho-parahydrogen conversion, thermoacoustic modeling.

Introduction

With growing efforts to achieve decarbonization of the energy industry (Griffiths et al. 2021), hydrogen is becoming an attractive energy carrier, as it can be produced by renewables and does not emit harmful pollutants when generating energy by reacting with oxygen. Hydrogen occupies large volumes when stored in the gaseous form, making utilization as a fuel for ground, aerial, and marine vehicles problematic. Liquid hydrogen has significantly better volumetric energy density, but low cryogenic temperatures are required for hydrogen liquefaction and liquid-form storage (Barron 1985).

Current methods for hydrogen liquefaction are rather inefficient (Radebaugh 2009), and little progress has been achieved in recent decades. Additional complication in this process is the necessity to convert hydrogen from predominantly the orthohydrogen spin-isomer form into the parahydrogen form (Pedrow et al. 2019). Without this conversion, which is very slow without assistance, liquid hydrogen storage suffers from large boil-off losses due to inevitable heat leaks. Effective ortho-parahydrogen conversion requires passing hydrogen through catalytic beds, additionally reducing efficiencies of hydrogen liquefaction systems.

¹ Corresponding author. Email: matveev@wsu.edu.

A conceptual way to improve cooling and conversion of cryogenic hydrogen was recently proposed (Matveev and Leachman 2022). This method involves thermoacoustic refrigerators where flowingthrough hydrogen serves as a working fluid and utilizes porous matrices not only for cooling but also for catalytic conversion taking advantage of the large surface area of porous stacks or regenerators. The name 'stack' is usually associated with a porous medium that has relatively large pore sizes (comparable to or greater than the acoustic thermal penetration depth) and is employed in standing-wave systems, while 'regenerators' commonly refer to matrices with much tighter pores ensuring very good thermal contact between gas and solid that are used in travelling-wave devices. Since this paper addresses mainly standing-wave setups, the term 'stack' is employed in the rest of the paper. Flow-through thermoacoustic cooling devices with stacks have been demonstrated in the past for ambienttemperature air (Reid and Swift 2000). Related to thermoacoustic systems, Stirling engines using hydrogen as a working gas but without mean flow were also considered (Dros 1965, Meijer 1970, Martini 1983), and performance improvements over helium systems were detected in certain operational ranges. Although traveling-wave thermoacoustic systems are generally known to have higher performance, the current analysis focuses on standing-wave setups, since standing-wave configurations are easier to construct and they may be better suited for systems with mean flow due to lower flow resistance in stacks with larger pore sizes. As this study serves as a foundational step for analysis of hydrogen in these basic systems, optimization of the acoustic phasing in a broad range, with inclusion of traveling-wave systems, is left for future work.

As the composition of the overall cooling system involving the conceived method for cooling hydrogen is not yet established, and will require long-term efforts, the present exploratory analysis focuses only on one component, namely a stack, where simultaneous cooling and transformation of hydrogen is assumed to take place over a modest temperature difference. Its schematic is shown in Fig. 1. The entire cooling system may also include acoustic sources, resonators, and possibly additional stacks or other cooling means to cover a large temperature range (e.g., from ambient to that of liquid hydrogen). Also, only a relatively small temperature difference across the stack in the vicinity of liquid nitrogen temperatures is considered in this study to keep the process relatively simple for two reasons: (1) future experimental comparisons with liquid nitrogen as a coolant, and (2) high sensitivity of the equilibrium orthohydrogen fraction to temperature in these conditions.

At the appropriate acoustic state, heat will be pumped in the considered setup (Fig. 1) by thermoacoustic phenomena from a low temperature space (at temperature T_C) to a high-temperature zone (at temperature T_H). In the superimposed mean flow from high- to low-temperature regions, hydrogen will experience cooling when passing through the stack. If the porous material is catalyzed, one can also achieve ortho-parahydrogen conversion from an ortho-rich state (e.g., normal hydrogen) to that with reduced ortho- fraction (due to decrease of equilibrium fraction at lower temperatures).

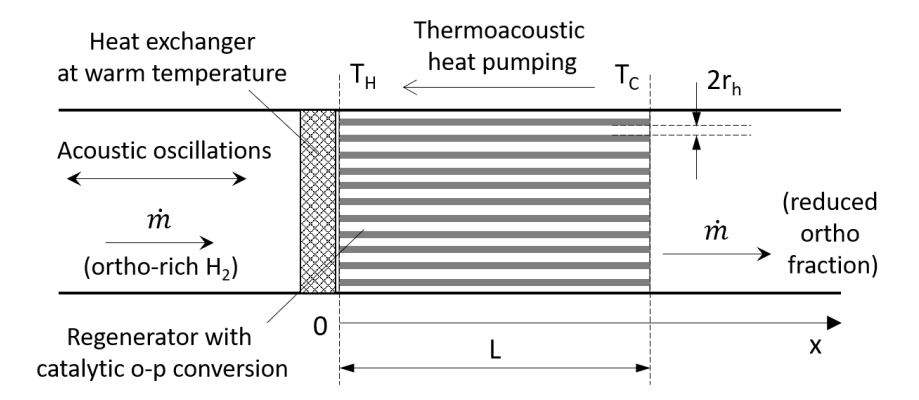


Fig. 1 Schematic of thermoacoustic stack for cooling and converting of hydrogen flow.

In the initial consideration of thermoacoustic-catalytic cooler for cryogenic hydrogen (Matveev and Leachman 2022), a simplistic lumped-element model with infinite-rate ortho-parahydrogen conversion was analyzed. To improve accuracy of the performance prediction for this device, the current study utilizes differential thermoacoustic equations that are integrated along the stack to describe variations of acoustic variables and mean temperature. In addition, an empirical catalytic reaction rate is employed to model ortho-parahydrogen conversion. Using this method, the present study investigates: (1) optimization of the stack geometry and placement inside the system, (2) comparison between catalyzed and non-catalyzed stacks with hydrogen and helium, and (3) performance sensitivity of the catalyzed setup to variations in operational conditions.

Modeling Approach

To analyze performance of a catalyzed stack and find favorable dimensions and operational conditions, the steady-state, low-amplitude, quasi-one-dimensional thermoacoustic model is applied. Acoustic fluctuations of pressure p' and volumetric velocity U' inside a stack are presented as follows,

$$p'(x,t) = Re[p_1(x)e^{i\omega t}], \tag{1}$$

$$U'(x,t) = Re[U_1(x)e^{i\omega t}], \qquad (2)$$

where $p_1(x)$ and $U_1(x)$ are complex amplitudes dependent on the longitudinal position x inside the stack (Fig. 1), ω is the angular frequency defined by the resonator properties or external power source, and t is the time.

The main governing equations include thermoacoustic forms of the continuity, momentum, and energy equations (Rott 1975, Swift 2002). For example, the momentum equation relates variation of the acoustic pressure amplitude to volumetric velocity magnitude and other system properties,

$$\frac{dp_1}{dx} = -\frac{i\omega\rho_m}{1 - f_v} \frac{U_1}{A},\tag{3}$$

where ρ_m is the mean fluid density, A is the cross-sectional area of the resonator occupied by the fluid, and f_v is the thermoacoustic function that accounts for viscous losses. Analytical expressions are available for this function in several regular geometries (Swift 2002); more complex porous media have also been analyzed (Matveev 2010). However, they are not drastically different, and for simplicity, the parallel-plate stack setup is considered in the present analysis, as illustrated Fig. 1. For this geometry, f_v is given as follows,

$$f_v = \frac{\tanh[(1+i)r_h/\delta_v]}{(1+i)r_h/\delta_v},\tag{4}$$

where r_h is the hydraulic radius or half-spacing between the plates (Fig. 1) and δ_v is the viscous penetration depth,

$$\delta_{v} = \sqrt{2\mu/(\omega\rho_{m})}, \tag{5}$$

where μ is the fluid viscosity.

The modified continuity equation gives an expression for the spatial evolution of the volumetric velocity amplitude,

$$\frac{dU_1}{dx} = -\frac{i\omega A_g}{\gamma p_m} \left[1 + (\gamma - 1) \frac{f_k}{\theta} \right] p_1 + \frac{f_k - f_v}{(1 - f_v)(1 - \sigma)(1 + \theta)} \frac{dT_m}{dx} \frac{U_1}{T_m}, \tag{6}$$

where γ is the ratio of specific heats, p_m and T_m are the mean pressure and temperature, respectively, σ is the Prandtl number, and f_k is another thermoacoustic function defined similar to Eq. (4), but with δ_v replaced by δ_k , the thermal penetration depth in the fluid,

$$\delta_k = \sqrt{2k/(\omega\rho_m c_p)} \,, \tag{7}$$

where k is the fluid thermal conductivity and c_p is the fluid specific heat capacity. The finite heat capacity of the solid is accounted for by parameter ε , defined as follows,

$$\theta = \frac{\rho_m c_p \delta_k \tanh[(1+i)r_h/\delta_k]}{\rho_s c_s \delta_s \tanh[(1+i)d/\delta_s]},\tag{8}$$

where ρ_s and c_s are the density and specific heat of the solid plate material, respectively, d is the plate half-thickness, and δ_s is the thermal penetration depth in the solid, defined similar to Eq. (7), but with solid material properties. The first term in Eq. (6), which includes dissipation, is common to conventional acoustic networks without a longitudinal temperature gradient, while the second term is the key to thermoacoustic phenomena. It can result in sound power generation or heat pumping from low- to high-temperature zones.

The thermoacoustic form of the energy equation can be written for the enthalpy flow \dot{H} along the stack (Swift 2002),

$$\dot{H} = \dot{E} + \frac{1}{2} Re \left[p_1 \widetilde{U}_1 \frac{\tilde{f}_v - f_k}{(1 + \sigma)(1 - \tilde{f}_v)(1 + \theta)} \right] + \dot{m}h + \left[\frac{\rho_m c_p |U_1|^2}{2\omega A(1 - \sigma^2)|1 - f_v|^2} Im \left(\widetilde{f}_v + \frac{(f_k - \tilde{f}_v)(1 + \theta f_v / f_k)}{(1 + \sigma)(1 + \theta)} \right) - (Ak + A_s k_s) \right] \frac{dT_m}{dx}, \tag{9}$$

where \dot{m} is the mean flow of hydrogen through the stack, h is the local enthalpy of hydrogen, A_s is the cross-sectional area of the resonator occupied by solid, and \dot{E} is the acoustic power flow,

$$\dot{E} = \frac{1}{2} Re \left[p_1 \widetilde{U}_1 \right]. \tag{10}$$

In stacks with commonly assumed adiabatic external walls, the enthalpy flow along the stack must remain constant. The enthalpy flow magnitude is defined by boundary conditions, e.g., by heat added or rejected at the upstream and downstream heat exchangers and acoustic power flows. Using $\dot{H}=const$, Eq. (9) can be brought to a form similar to Eqs. (3,6) with dT_m/dx term on the left-hand side.

The three governing equations, Eqs. (3,6,9), can be numerically integrated along the x-direction to find acoustic amplitudes and mean temperature, which will define pumped heat (or cooling power), consumed acoustic power, and other performance characteristics of the stack. One novel feature in the present analysis is that the hydrogen enthalpy h, which appears in Eq. (9), depends not only on a local

temperature but also on a local orthohydrogen fraction. This fraction will vary along x in the case of a catalyzed stack.

To model the catalytic ortho-parahydrogen conversion, an empirical equation for the variation rate of the orthohydrogen fraction y_0 is employed here based on the data reported by Zhuzhgov et al. (2018),

$$\frac{dy_o}{dx} = (y_{o,eq} - y_o) \frac{k_v M A_s}{m},\tag{11}$$

where $y_{o,eq}$ is the local equilibrium fraction of orthohydrogen fraction that depends on temperature (Fig. 2), M is the molar mass of hydrogen, and k_v is the conversion rate constant. In the present study, the value of k_v is selected as 0.0025 mol/(cm³s), which corresponds to the upper range of experimental results available for this parameter at temperatures similar to those in the present study (Zhuzhgov et al. 2018). Thus, in addition to Eqs. (3,6,9), Eq. (11) is also numerically integrated along the stack starting with an initial orthohydrogen fraction at the inlet (warm) side.

Important metrics of stacks, reported in the next section, include the coefficient of performance and the second-law efficiency,

$$COP = \frac{m(h_W - h_C)}{\dot{E}_W - \dot{E}_C},\tag{12}$$

$$\eta_{II} = COP \frac{T_W - T_C}{T_C},\tag{13}$$

where subscripts w and c stand for the warm (inlet) and cold (outlet) ends of the stack, respectively. In Eq. (12), the nominator is the heat removed from the flowing hydrogen, and the denominator is the acoustic power consumed inside the stack. In Eq. (13), this coefficient of performance is divided by the Carnot COP. The inlet (warm) quantities in Eqs. (12,13) are given inputs in this study, while the outlet (cold) properties are calculated upon numerically integrating Eqs. (3,6,9,11) along the stack. The fluid properties are obtained from CoolProp software (Leachman et al. 2009, Bell et al. 2014).

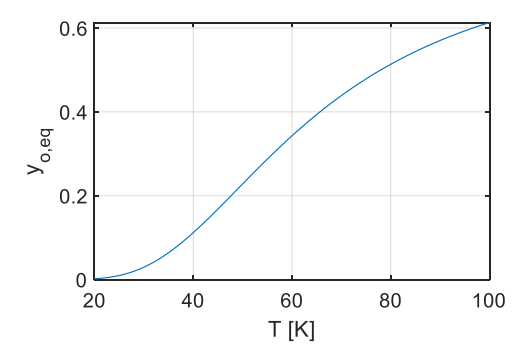


Fig. 2 Equilibrium fraction of orthohydrogen.

Results

The selection of conditions favorable for cooling and ortho-parahydrogen conversion of flowing-through hydrogen can be accomplished using thermoacoustic theory with an addition of conversion rate of hydrogen. The ortho-parahydrogen conversion is accompanied by heat release and therefore additional heat load inside the stack. The base parameters for the configuration outlined in Fig. 1 and analyzed here are listed in Table 1. These parameters are selected as suitable for laboratory experimentation and possibly for practical use in larger systems with more components. The temperature at the stack inlet is chosen as 80 K, implying that some pre-cooling will be done either thermoacoustically with additional

stacks or employing other methods, e.g., using liquid nitrogen. While these parameters can be optimized for specific applications, most of them are fixed in the present study. It should be noted that the mean mass flux, stands for the time-averaged component of the flow and not the oscillatory acoustic flow.

Table 1 Base parameters of hydrogen flow-through stack setup and inlet conditions.

Stack length	20 cm
Stack porosity	0.5
Solid material	Stainless steel
Mean pressure	5 bar
Mean mass flux	0.15 kg/(s-m ²)
Acoustic frequency	100 Hz
Inlet (warm) temperature	80 K
Inlet orthohydrogen fraction	0.75
Inlet acoustic power flux	15 kW/m ²
Outlet/inlet acoustic power ratio	0.15

The first parametric study is determine favorable values for the plate half-spacing (hydraulic radius r_h) and position of the stack inside the entire system, which can be characterized by the absolute value of normalized acoustic impedance z at the warm side of the stack,

$$z = \frac{|p_1|A_{res}}{|U_1|\rho_m c},\tag{14}$$

where A_{res} is the resonator cross-sectional area (upstream of the stack) and c is the speed of sound. The impedance variation can be achieved using adaptable acoustic networks (Matveev et al. 2006).

The calculation procedure is arranged as follows. First, the inlet acoustic pressure amplitude is guessed. Then, the acoustic velocity magnitude is determined from the given inlet impedance magnitude (Eq. 14), and the phase between the acoustic pressure and velocity is found from the given inlet acoustic power. Upon integrating the thermoacoustic equations along the stack, the outlet acoustic power is calculated. If it differs from the specified power (15% of the inlet power) by more than a tolerance value (0.1% of the inlet power), then another inlet pressure magnitude is selected, and the calculations are repeated. These iterations continue until the outlet-to-inlet power ratio is within the acceptable tolerance.

The results of parametric calculations for the achieved cold temperature of the hydrogen flow, pressure amplitude upstream of the stack, the coefficient of performance (Eq. 12), and the second law efficiency (Eq. 13) are illustrated in Fig. 3 for the catalyzed system. The COP values exhibit saturation trends in wider channels, as the thermal penetration becomes sufficiently smaller than the plate spacing, and the channel enter the so-called boundary-layer regime. With additional constraints including cold temperatures below 70 K and acoustic pressure amplitudes below 15% of the mean pressure (to minimize nonlinear acoustic losses in the resonator), the hydraulic radius of $r_h = 0.4$ mm and impedance of z = 6 can be selected. These values correspond to the stack COP and second-law efficiency close to their maxima in the parametric range under the chosen constraints.

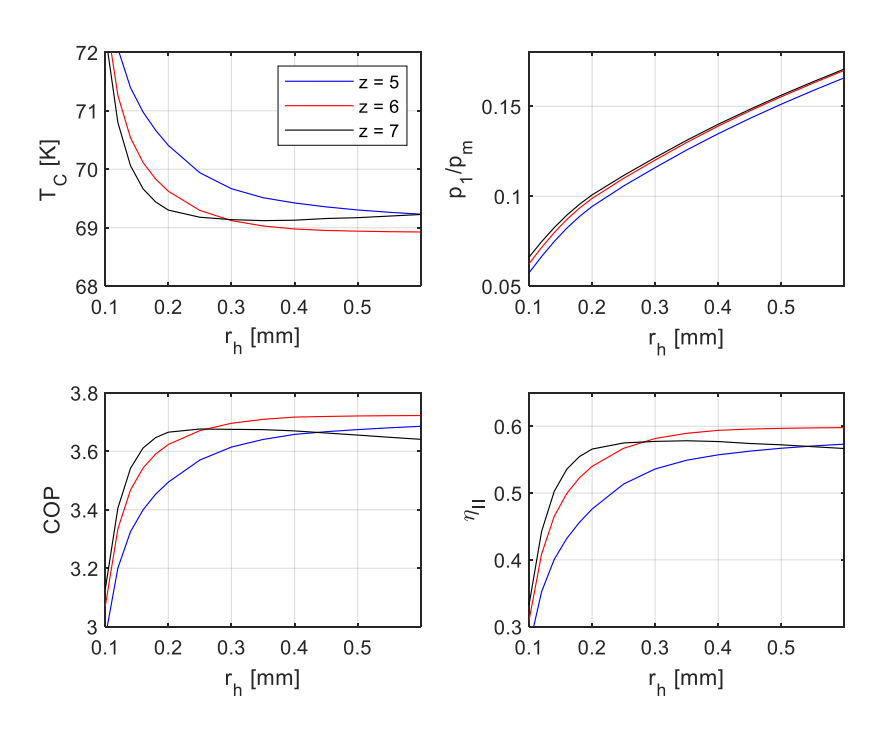


Fig. 3 Performance characteristics of a catalyzed stack at variable hydraulic radius and normalized acoustic impedance.

It is instructive to compare performance of catalyzed and non-catalyzed stacks, we well as a system using helium, which is a commonly used working gas in cryocoolers. Calculations for these two additional setups were conducted in similar operational conditions as for the catalyzed stack with hydrogen, and an acoustic impedance and half-plate spacing were again used as variable parameters. Flow rates for helium and hydrogen in the non-catalyzed stacks were adjusted to values 0.49 and 0.30 kg/m², respectively, in order to attain the same outlet cold temperature of about 69 K. The obtained results for these two setups are shown in Fig. 4. Although general trends are the same as in the previous case, significant performance reductions are observed for the non-catalyzed hydrogen and helium cases. The hydrogen-filled non-catalyzed stack has both COP and η_{II} about 25% lower than the catalyzed case, whereas the optimized helium system shows about 45% degradation of these metrics. As the consumed acoustic power is the same for all three cases, the COP in Figs. 3 and 4 is directly proportional to removed heat, thus showing substantially larger cooling capacity of the catalyzed system.

Higher performance of hydrogen over helium system can be related to higher specific heats and speed of sound of hydrogen, which are thermoacoustically advantageous, while viscosity of hydrogen is lower than that of helium, which leads to lower viscous losses. When comparing two hydrogen cases with catalyzed and non-catalyzed stacks, the effective heat load in the catalyzed system is higher at the warm side (due to ortho-rich hydrogen entering the stack and being converted to parahydrogen), while in the non-catalyzed system the maximum heat load appear near the cold side of the stack, as shown later in Fig. 7a. As it is more efficient to remove heat at warmer temperature, the catalyzed system COP becomes greater. The present findings indicate that catalyzed stacks with hydrogen as a working fluid may potentially improve efficiencies of thermoacoustic cryocoolers, although one should keep in mind that this study focuses on a rather specific setup that differs from traditional cryocoolers.

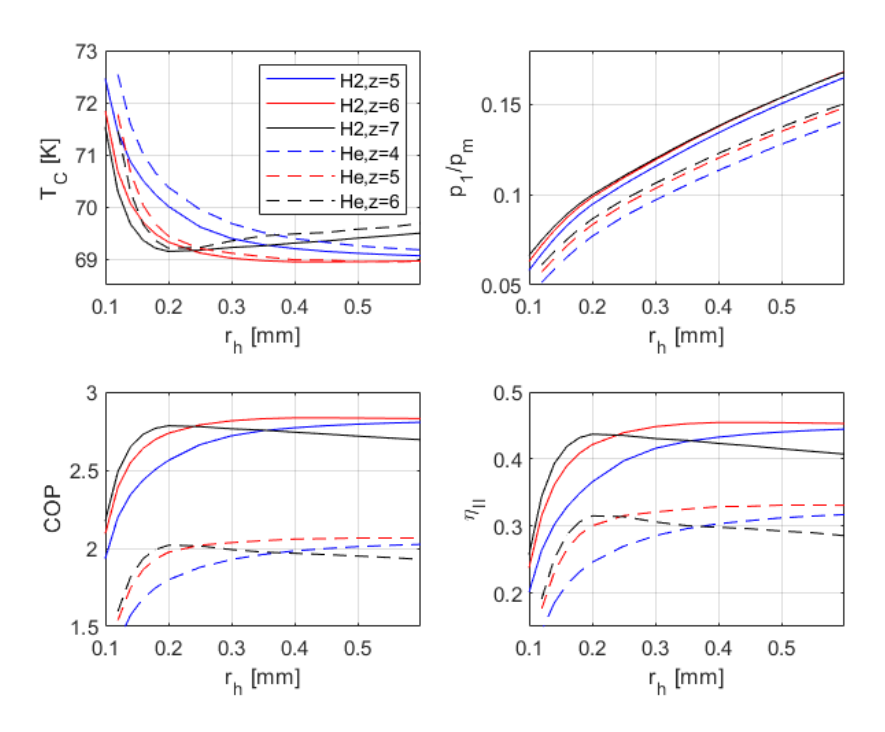


Fig. 4 Performance characteristics of non-catalyzed stacks with hydrogen and helium at variable hydraulic radius and normalized acoustic impedance.

More detailed information about thermal and acoustic characteristics inside hydrogen-filled stacks at the selected optimal condition (r_h = 0.4 mm and z = 6) is provided in Figs. 5-7. The acoustic pressure and velocity amplitudes are shown in Fig. 5. The reference phase for the acoustic pressure at the stack inlet is chosen as zero, whereas the acoustic velocity fluctuations lag the pressure oscillations by slightly less 90 degrees (to provide acoustic energy flow into the stack). The variations of acoustic amplitudes in the considered stack are relatively modest.

As shown in Fig. 6, the hydrogen temperature decreases towards the outlet side, since thermoacoustic processes pump heat upstream. In the catalyzed case with mean flow, the temperature does not drop immediately near the entrance due to exothermic conversion of ortho-rich hydrogen entering the stack. Otherwise, temperature profiles in the catalyzed and non-catalyzed systems with mean flow are similar. Also plotted in Fig. 6 is the temperature distribution in the non-catalyzed stack without mean flow (shown by a dash-dotted line). Since thermoacoustic heat pumping does not need to remove heat from flowing-through hydrogen in this situation, the temperature drop along the stack is larger.

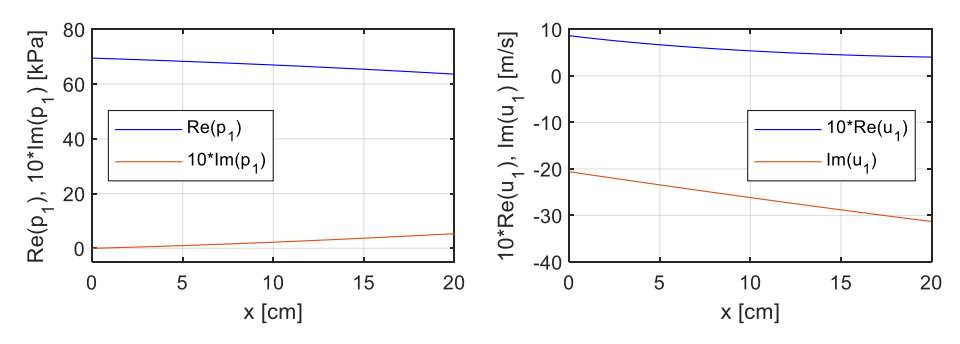


Fig. 5 Real and imaginary components of acoustic pressure and velocity amplitudes in the stack.

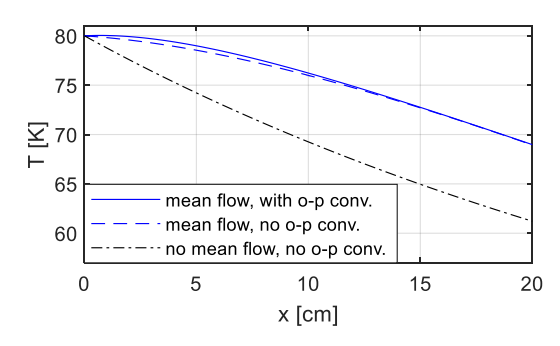


Fig. 6 Mean temperature distribution in the stack with and without mean flow.

The effective volumetric heat source q, defined here as the heat removed from hydrogen per unit volume, is given in Fig. 7 for the optimal condition with mean flow. Plotted in this figure, q_{tot} stands for the total heat density removal rate, including heat released due to ortho-parahydrogen conversion and cooling hydrogen flow, whereas q_{op} accounts only for the conversion. In the case with orthoparahydrogen conversion, it is maximized near the warm inlet side, where the normal hydrogen is undergoing intensive conversion at the large difference between local and equilibrium orthohydrogen fractions, y_o and $y_{o,eq}$ (Fig. 7). The overall ortho-parahydrogen conversion heat in the stack slightly exceeds the sensible heat. In the case with no reaction, more heat is removed from flowing hydrogen towards the colder exit, which contributes to lower efficiency of the non-catalyzed setup (Fig. 3). The equilibrium fractions of orthohydrogen diminish along the stack (Fig. 7). In the situation with orthoparahydrogen conversion, the orthohydrogen fraction y_o is approaching the equilibrium value $y_{o,eq}$, but does not quite reach the equilibrium composition due to the finite rate of conversion and the limited size of stack.

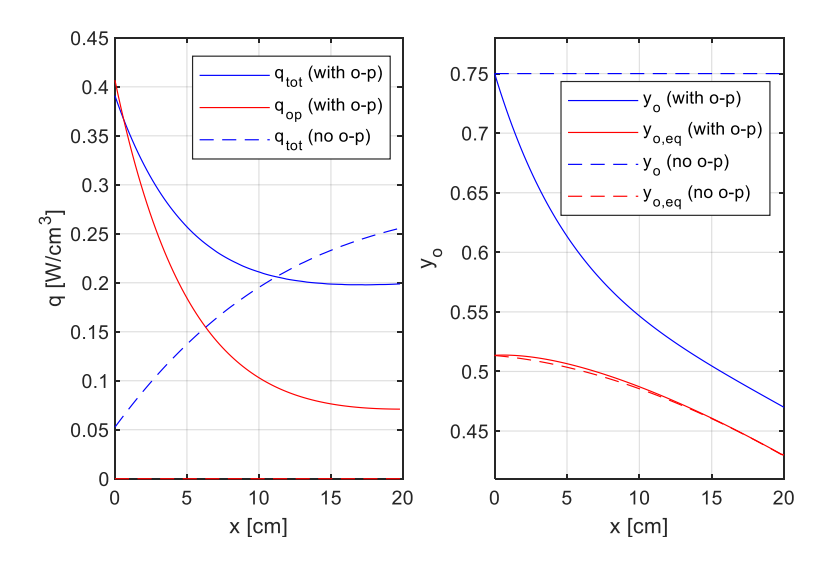


Fig. 7 Distribution of effective heat sources and orthohydrogen fraction along the stack with mean flow.

Additional results have been obtained with different stack lengths and mean pressure in otherwise the same system with ortho-parahydrogen catalyzed conversion (Fig. 8). At the same mean pressure and hydrogen flow-through rate (blue line in Fig. 8), the stack length resulting in lower outlet temperature, as well as higher COP and second-law efficiency, is found to be shorter than in the previously considered example. However, reduced length also leads to increasing acoustic pressure amplitude and may result in large acoustic losses in other parts of the system.

A possible variation of operational conditions in the catalyzed-stack system with hydrogen may include lower mean pressure. Results obtained for 1-bar case with the same acoustic power input and mean flow rate are included in Fig. 8 (red line). This operational mode leads to less significant cooling, lower performance metrics, and substantially higher requirements for the acoustic pressure amplitude. Such detrimental effects can be mitigated by lowering acoustic power and hydrogen flow (black line in Fig. 8). Efficiency indicators noticeably increase and both cold temperature and pressure amplitude decrease in this case. However, this improvement comes at much lower throughput of cooled hydrogen.

Results for broader variations of mass flow rate and supplied power in the original 5-bar catalyzed system with hydrogen are given in Fig. 9. Naturally, larger supplied power leads to lower outlet temperatures, while increasing acoustic pressure amplitude. The higher flow rate of hydrogen leads to smaller temperature drop, whereas acoustic amplitudes are decreased. The coefficient of performance tends to increase at lower acoustic power and larger flow rate in the studied range, while peaks in the second-law efficiency manifest shifts to higher flow rates at increasing acoustic power.

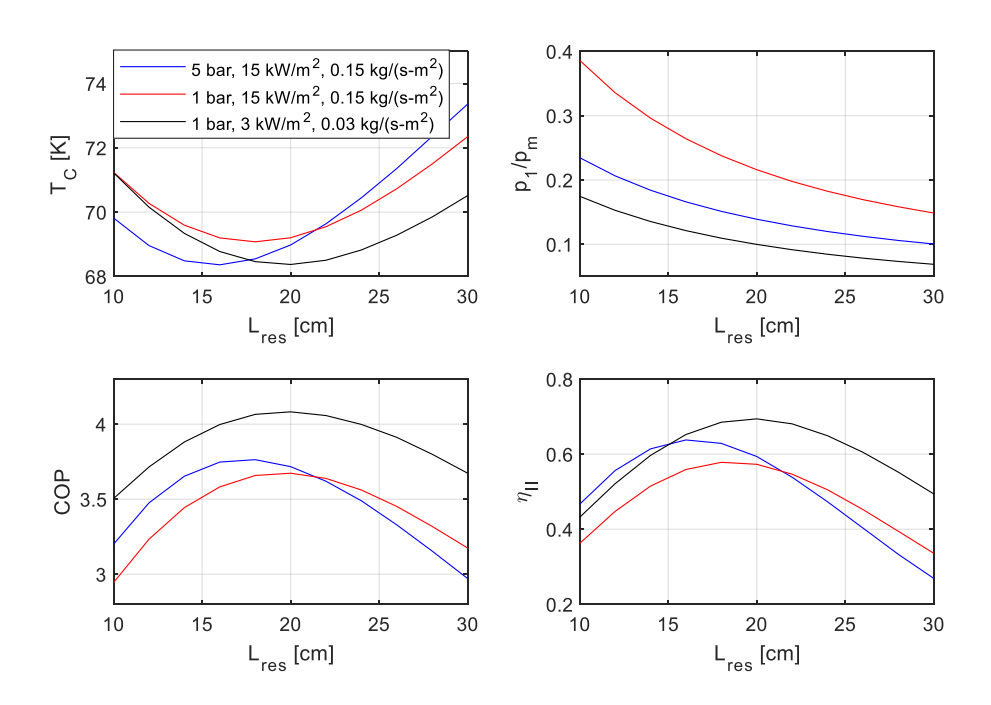


Fig. 8 Performance characteristics of catalyzed stack at variable stack length and mean pressure.

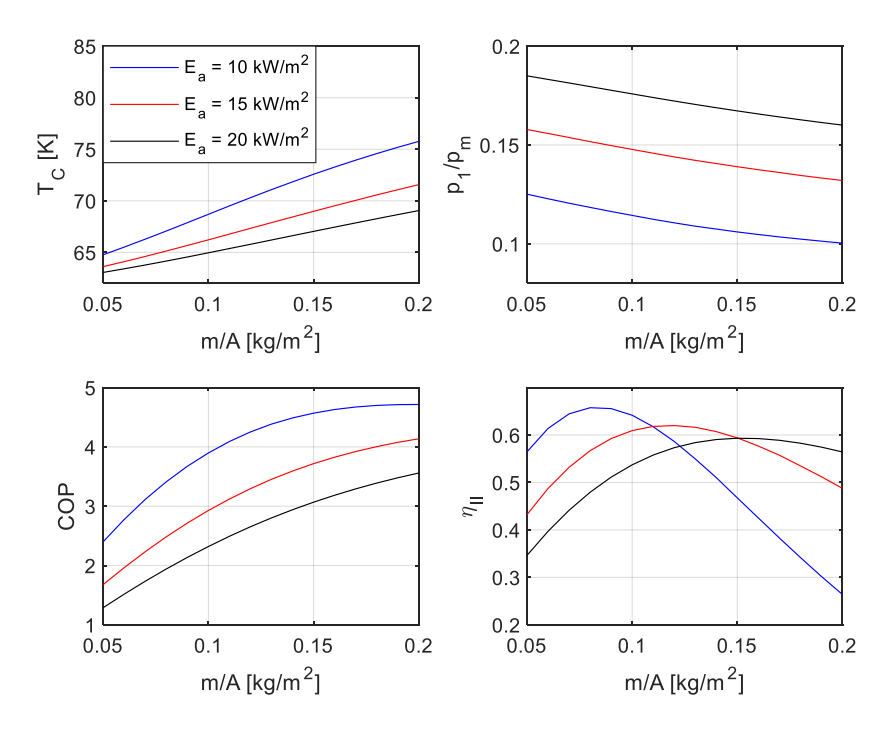


Fig. 9 Performance characteristics of catalyzed stack at variable hydrogen flow rate and supplied acoustic power.

Conclusions

To model a novel method for simultaneous cooling and transforming cryogenic hydrogen in a catalyzed porous medium, a one-dimensional thermoacoustic model for a stack has been augmented with a reaction describing catalytic ortho-parahydrogen conversion of flowing hydrogen. A limited optimization of the stack geometry and its placement inside a resonator was demonstrated to achieve significant cooling of hydrogen at the second-law stack efficiencies near 0.6. Performance advantages of approximately 25% and 45% were found for the optimized catalyzed stack relative to optimized non-catalyzed stacks with hydrogen and helium, respectively. This implies that use of hydrogen could outperform helium as the working fluid of a cryocooler in some operational regimes, and thereby reduce reliance on helium as a non-renewable resource. Distributions of temperature, heat removed from the flow, and orthohydrogen-fraction in the hydrogen system show that most intensive heat exchange and conversion occur in the front portion of the catalyzed stack when normal hydrogen enters the catalyzed medium at cryogenic temperature. Variations of mean pressure and flow rate of hydrogen will require adaptation of supplied acoustic power to maintain efficient operation in the same system.

Future work on this topic should focus on experimental testing and optimization of catalyzed stacks and entire cooling systems, including consideration of traveling-wave setups, manufacturing stacks of optimal geometries, catalyst deposition, and efficacy of ortho-parahydrogen catalytic conversion in acoustic flow. Numerical modeling of more complex systems involving larger temperature differences in longer stacks with variable properties will be important for optimizing practical systems.

Acknowledgement

This work was supported in part by the U.S. National Science Foundation under Grant No. 2214235.

References

Barron, R.F., 1985. Cryogenic Systems, Oxford University Press, New York.

Bell, I.H., Wronski, J., Quoilin, S., Lemort, V., 2014. Pure and pseudo-pure fluid thermophysical property evaluation and the open-source thermophysical property library CoolProp, Industrial & Engineering Chemistry Research, 53 (6), 2498-2508.

Dros, A.A., 1965. An industrial gas refrigerating machine with hydraulic piston drive, Philips Technical Review, 26, 297-308.

Griffiths, S., Sovacool, B.K., Kim, J., Bazilian, M., Uratani, J.M., 2021. Industrial decarbonization via hydrogen: a critical and systematic review of developments, socio-technical systems and policy options, Energy Research & Social Science, 80, 102208.

Leachman, J.W., Jacobsen, R.T., Penoncello, S.G., Lemmon, E.W., 2009. Fundamental equations of state for parahydrogen, normal hydrogen, and orthohydrogen, J. Phys. Chem. Ref. Data, 38 (3), 721–748.

Martini, W., 1983. Stirling Engine Design Manual, NASA Report CR-158088.

Matveev, K.I., Swift, G.W., Backhaus, S., 2006. Temperatures near the interface between an ideal heat exchanger and a thermal buffer tube or pulse tube, International Journal of Heat and Mass Transfer, 49, 868-878.

Matveev, K.I, 2010. Thermoacoustic energy analysis of transverse-pin and tortuous stacks at large acoustic displacements, International Journal of Thermal Sciences, 49, 1019-1025.

Matveev, K.I., Leachman, J.W., 2022. Thermoacoustic flow-through cooler for cryogenic hydrogen, Computer Aided Chemical Engineering, 49, 1891-1896.

Meijer, R.J., 1970. Prospects of the Stirling engine for vehicular propulsion, Philips Tech. Rev., 31, 168-185.

Pedrow, B.P., Muniyal Krishna, S.K., Shoemake, E.D., Leachman, J.W., Matveev, K.I., 2021. Parahydrogen—orthohydrogen conversion on catalyst-loaded scrim for vapor-cooled shielding of cryogenic storage vessels, Journal of Thermophysics and Heat Transfer, 35, 142-151.

Radebaugh, R., 2009. Cryocoolers: the state of the art and recent developments, J. Phys.: Condens. Matter, 21, 164219.

Reid, R.S., Swift, G.W., 2000. Experiments with a flow-through thermoacoustic refrigerator, Journal of the Acoustical Society of America, 108, 2835-2842.

Rott, N., 1975. Thermally driven acoustic oscillations, part III: second-order heat flux, Z. Angew. Math. Phys., 26, 43-49.

Swift, G.W., 2002, Thermoacoustics: a Unifying Perspective for Some Engines and Refrigerators, Acoustical Society of America, Melville, NY, USA.

Zhuzhgov, A.V., Krivoruchko, O.P., Isupova, L.A., Mart'yanov, O.N., Parmon, V.N., 2018. Low-temperature conversion of ortho-hydrogen into liquid para-hydrogen: process and catalysts. Review, Catalysis in Industry, 10 (1), 9–19.